Published in final edited form as:
Structure. 2009 August 12; 17(8): 1082–1091. doi:10.1016/j.str.2009.06.003.

The structure of the scaffold nucleoporin Nup120 reveals a new and unexpected domain architecture

Nina C. Leksa[1,2], **Stephen G. Brohawn**[1,2], and **Thomas U. Schwartz**[1,*]

[1]Department of Biology, Massachusetts Institute of Technology 77 Massachusetts Avenue, Cambridge, MA 02139, USA

SUMMARY

Nucleocytoplasmic transport is mediated by nuclear pore complexes (NPCs), enormous protein assemblies residing in circular openings in the nuclear envelope. The NPC is modular, with transient and stable components. The stable core is essentially built from two multiprotein complexes, the Y-shaped heptameric Nup84 complex and the Nic96 complex, arranged around an eightfold axis. We present the crystal structure of $Nup120_{1-757}$, one of the two short arms of the Y-shaped Nup84 complex. The protein adopts a compact oval shape built around a novel bipartite α-helical domain intimately integrated with a β-propeller domain. The domain arrangement is substantially different from the Nup85•Seh1 complex, which forms the other short arm of the Y. With the data presented here we establish that all three branches of the Y-shaped Nup84 complex are tightly connected by helical interactions and that the β-propellers likely form interaction site(s) to neighboring complexes.

INTRODUCTION

The main feature that distinguishes eukaryotes from prokaryotes is the confinement of the genetic material into a membrane-enveloped nucleus. Since gene transcription and mRNA processing occur inside the nucleus while protein translation is restricted to the cytoplasm, transport across the double-layered nuclear envelope (NE) is essential for cellular homeostasis. The exchange of all molecules, including ions, proteins, and RNAs is facilitated exclusively by nuclear pore complexes (NPCs) (D'Angelo and Hetzer, 2008; Lim et al., 2008; Tran and Wente, 2006; Weis, 2003). NPCs are large protein assemblies of 40-60 MDa that are embedded in the nuclear envelope and exhibit an 8-fold rotational symmetry around a central axis in addition to an imperfect two-fold symmetry across the plane of the NE (Beck et al., 2007; Stoffler et al., 2003). Composed of multiple copies of ~ 30 proteins, termed nucleoporins (nups), the NPC has an outer diameter of ~100 nm while the central channel measures ~40 nm in width. Transmembrane nups directly connect the NPC to the NE, while the phenylalanine-glycine (FG) repeat-containing Nups line the interior of the pore. These FG-filaments mediate nucleocytoplasmic transport of cargo molecules across the NE. FG-filament bearing nups are anchored to the NPC scaffold built from architectural nucleoporins arranged in two large

*Correspondence: tus@mit.edu.

[2]These authors contributed equally to this work

ACCESSION NUMBER

The atomic coordinates of the Nup120 structure have been deposited in the Protein Data Bank (PDB) with accession number 3HXR.

multiprotein complexes that form a membrane-proximal layer. The scaffold structure is very stable and undergoes virtually no turnover in the quiescent cell (D'Angelo et al., 2009), while many other nucleoporins have variable dwell times at the NPC (Rabut et al., 2004). In consequence, the NPC is a highly modular structure (Schwartz, 2005). Understanding the structure of the NPC therefore depends upon elucidating its basic scaffold.

The two essential architectural building blocks of the NPC are the Nup84 subcomplex and the Nic96 subcomplex. The components of the Nic96 subcomplex likely include Nic96, Nup53/59, Nup157/170, Nup188 and Nup192 (yeast nomenclature), as inferred from co-immunoprecipations (co-IPs) (Alber et al., 2007; Hawryluk-Gara et al., 2008; Marelli et al., 1998; Onischenko et al., 2009) and yeast-two-hybrid screens (Wang et al., 2009; Yu et al., 2008). Judged by immunolabeling, the Nic96 subcomplex might form a central ring within the NPC sandwiched between peripheral rings formed by Nup84 subcomplexes (Alber et al., 2007). In comparison to the Nic96 subcomplex, the Nup84 subcomplex is substantially better understood. It has 7 universally conserved members (yeastNup84/humanNup107, yNup85/hNup75, yNup120/hNup160, Nup133, yNup145C/hNup96, Sec13, and Seh1) and three additional members (Nup37, Nup43, and ELYS/Mel-28) to date found mainly in metazoa (Cronshaw et al., 2002; Gillespie et al., 2007; Loiodice et al., 2004; Rasala et al., 2006). In the fungus *Aspergillus nidulans*, distant Nup37 and ELYS orthologs have been described recently (Liu et al., 2009). The heptameric core Nup84 complex assembles tightly as shown by co-IPs and *in vitro* assembly (Harel et al., 2003; Lutzmann et al., 2002; Siniossoglou et al., 2000; Walther et al., 2003). Negatively-stained electronmicrographs of the assembled Nup84 complex reveal a branched Y-shaped structure, with two short arms and a kinked stalk connected at a central hub (Lutzmann et al., 2002).

Crystallographic analysis of the Y-complex has progressed quickly. The kinked stalk ends with a flexibly attached β-propeller domain (Berke et al., 2004) at the N-terminus of Nup133 followed by an irregular C-terminal helical stack domain that connects end-to-end to Nup84 (Boehmer et al., 2008); Whittle, unpublished). The Nup84•Nup133 interface defines at least one kink in the stalk. The opposite end of Nup84 links to Nup145C (Brohawn et al., 2008). Nup145C•Sec13 (Hsia et al., 2007) resides proximal to the hub (Lutzmann et al., 2002). Nup85•Seh1 forms one of the two short arms of the Y-shaped complex (Brohawn et al., 2008; Debler et al., 2008). Nup84, Nup85, and Nup145C are structurally related (Brohawn et al., 2008), despite very low sequence conservation, as are the β-propeller proteins Seh1 and Sec13.

Nup120 is the last remaining Y-complex component without structural information. Here we report the 3.0 Å crystal structure of Nup120 (residues 1-757 of 1037), which reveals a compact and rigid structure composed of an N-terminal β-propeller domain tightly integrated into a novel bipartite α-helical domain. Our structure largely defines the second short arm of the Y-complex. Comparison with other members of the Y-complex, phylogenetic analysis, *in vitro* binding experiments, and *in vivo* localization data suggest a role for Nup120 consistent with our lattice-like model of the NPC.

RESULTS

Structure Determination

After systematic C-terminal truncation, a stable fragment comprising most of Nup120 (residues 1-757 of 1037 total) from *S. cerevisiae* was recombinantly expressed in *E. coli* and purified. The protein is a monomer in solution (data not shown). Native protein readily crystallized and selenomethionine derivatized crystals were obtained after microseeding with native crystals. Though both crystal forms were optically identical, the selenomethionine crystals diffracted better and were used exclusively in structural analysis. The structure of Nup120 was solved

with one molecule per asymmetric unit by single-wavelength anomalous dispersion (SAD) on very strong Se-Peak data (all 9 Se sites are well ordered). The model is complete except for 27 residues at the C-terminus and 7 flexible loops (out of 43 total loops) and was refined to R_{work} / R_{free} of 24.4 % / 29.9 % (Table 1).

Crystal Structure of Nup120

Nup120 folds into a continuous, prolate disk with overall dimensions of 90 Å × 55 Å × 35 Å. One half of the structure is formed by an N-terminal β-propeller domain that is intimately connected to a compact central domain built from two closely packed α-helical segments (Figure 1). Overall, the structure is better resolved in the α-helical segment than the β-propeller, likely a result of a paucity of packing contacts involving the latter. The β-propeller of Nup120 contains 7 consecutive blades that fan out from a central axis. The blades are formed by a β-sheet of 4 consecutive antiparallel strands, labeled A-D. Blade 7 is built from the very N-terminus of the polypeptide chain forming strand 7D and joining strands 7A-C to close the propeller in a velcro-like closure commonly observed in β-propeller domains (Chaudhuri et al., 2008). Blade 1 is 5-stranded, with strand 7D extending to form the additional strand 1E before connecting to strand 1A (Figure 1E). Blade 3 is somewhat unusual in that the outermost strand 3D is only loosely connected to strand 3C with a hydrogen-bonding network hardly visible in our structure and the sequence could only be tentatively assigned for strand 3D residues 204-216.

The α-helical domain that forms the second half of the molecule is constructed in a unique discontinuous manner. In total the domain contains 15 helices, labeled α1-α15. The first 4 helices form a compact bundle and are inserted between blades 6 and 7 of the β-propeller. The remaining 11 helices are C-terminal to the β-propeller and pack tightly against the 4-helix bundle to form one compact entity. The arrangement of the helices is highly irregular. The most prominent feature of the domain are two long helices, α11 and α12, which pack against each other and form a central stalk, defining the long axis of the domain. Helices α5-α9 wrap up and around this element, with helices α6/α7 and α8/α9 arranged in two stacked braces oriented perpendicular to the stalk. Helices α1, and α13-α15 meander back down and around the other side to bury most of the hydrophobic stalk. The remaining surface area of the two central helices is closed by the 4-helix insertion bundle. Taken as a whole, the structure of $Nup120_{1\text{-}757}$ consists of a bipartite helical domain that is interrupted by a β-propeller.

The Main Crystal Contact is Formed by a Domain Swap

Other than a collection of spurious small contacts crystal packing is mainly achieved by a domain swap of the terminal helices α15 and α15′ exchanging between two neighboring molecules (Figure 2A). The interface measures 1355 $Å^2$, is entirely hydrophobic and highly complementary (Figure 2B). Domain swaps are regularly found in crystals (Liu and Eisenberg, 2002) and, as stated above, we do not observe dimerization of Nup120 in solution. We cannot rule out the possibility that the interface is physiologically relevant; sterically the domain swap is conceivable in the context of the entire molecule including the C-terminal 280 residues omitted in our construct. It is however more likely that the exposed hydrophobic patch is artificially generated by the truncation of the domain, since we also do not observe particularly high sequence conservation within helix α15. We speculate that *in vivo* the patch likely accommodates one of the additional helices from the C-terminal domain, or alternatively, is involved in interaction with a neighboring molecule. Whether the C-terminal domain is rigidly or flexibly tethered to Nup1201-757 is an open question.

Conservation of Nup120 and Comparison to the Human Ortholog Nup160

Overall, sequence conservation between Nup120 orthologs is weak as is typically observed in scaffold nucleoporins (Brohawn et al., 2008; Jeudy and Schwartz, 2007). Most of the better-

conserved residues are buried in the hydrophobic core of the protein and are involved in maintaining the structural integrity of the protein. On the protein surface we find few conserved patches (Figure 3A). Most distinct is an area on the edge of the β-propeller, corresponding to the outer strands of blade 3 and the loop leading into blade 4. The conserved sequence begins in the 3BC loop and continues into strand 3C itself. Although generally buried in canonical β-propellers, here strand 3C is quite exposed. This is probably the result of weaker interactions with strand 3D, which is flanked by two large loops and peels away from the core of the propeller. Additional conserved residues are spotted around this area, creating a relatively large conserved patch. The potential significance of this observation is discussed below.

We analyzed the charge distribution on the surface of Nup120 (Figure 3B). Since Nup120 is part of the scaffold structure of the NPC, we asked whether it may be possible that it directly juxtaposes the pore membrane. This would also be consistent with a membrane-curvature sensing ALPS motif, predicted in helix α5-6 of Nup120 (Drin et al., 2007). The surface charge of $Nup120_{1\text{-}757}$, however, is fairly mixed without conserved positive patches that might suggest direct membrane interaction. The ALPS motif is embedded in the structure and it is rather unlikely that it would swing out and insert in the membrane. Thus we suggest that $Nup120_{1\text{-}757}$ does not directly touch the nuclear membrane.

Structure-guided sequence comparison of Nup120 and its human ortholog Nup160 strongly suggests that both proteins adopt the same unique fold despite a low sequence identity of ~10 %. Both non-canonical characteristics of Nup120 (the helical insertion between blades 6 and 7 of the N-terminal β-propeller and the long central stalk helices forming the hydrophobic core of the central domain) are clearly conserved in Nup160. The 279 additional residues of Nup160 are dispersed over several regions and mostly correspond to different loop lengths connecting α-helices and β-strands. Of note, the C-terminal domain of Nup160, which is not present in the Nup120 crystal structure described here, has 5 additional predicted helices, possibly indicating a vertebrate-specific extension. Despite these differences, the Nup120 crystal structure is likely generally representative of all Nup120/Nup160 orthologs.

The C terminus of Nup120 Directly Binds Nup145C and Nup85

We sought to map the interaction of Nup120 with its direct binding partners in the Y-complex, Nup145C and Nup85. In a gel filtration assay, we tested for the formation of a pentameric Sec13•Nup145C•Nup120•Nup85•Seh1 complex (Figure 4). Incubating $Nup120_{766\text{-}1037}$ or $Nup120_{1\text{-}757}$ with both Nup145C• Sec13 and Nup85•Seh1 resulted in complex formation only for the C-terminal Nup120 domain, but not for the crystal construct. In combination with previous interaction mapping experiments (Brohawn et al., 2008), we conclude that the helical tails of the ACE1 domains of both Nup145C and Nup85 each interact directly with the helical $Nup120_{766\text{-}1037}$. This positions the C-terminus of Nup120 at the center of the hub of the Y-complex.

Without its C-terminal domain Nup120 does not properly localize to the NPC

Having established that $Nup120_{766\text{-}1037}$ is sufficient to bind both Nup145C• Sec13 and Nup85•Seh1 *in vitro*, we sought to examine the integration determinants of Nup120 into the NPC *in vivo*. *NUP120* is not essential in yeast but *nup120 Δ* cells exhibit a pore clustering phenotype (Aitchison et al., 1995; Heath et al., 1995) that is reminiscent of but less severe than the pore clustering observed for other scaffold nucleoporins including Nup84 and Nup133 (Li et al., 1995; Pemberton et al., 1995; Siniossoglou et al., 1996). We genomically GFP-tagged full length Nup120 and replaced the C-terminal 280 residues of genomic Nup120 with an in frame GFP-tag to create strains expressing Nup120-GFP or $Nup120_{1\text{-}757}$-GFP in a BY4741 background and examined the localization of the proteins via immunofluorescence (Figure 5). Nup120-GFP properly localizes to the NPC and shows typical nuclear rim staining,

superimposing well with mAb414-staining of FG-Nups (Aris and Blobel, 1989). $Nup120_{1-757}$-GFP, on the other hand, does not properly localize to the nuclear envelope and shows staining throughout the cell. This result is consistent with our *in vitro* data and suggests that the integration into the Y-complex is important for proper localization of Nup120.

Nup120 is Topologically Different from other Scaffold Nucleoporins

A recent surge in the X-ray crystallographic analysis of components of the NPC has greatly increased the repertoire of available structures of nucleoporins constituting the structural scaffold of the NPC. These structures (including those of Nic96 (Jeudy and Schwartz, 2007; Schrader et al., 2008), Nup133-NTD (Berke et al., 2004), Nup133•Nup107 interaction complex (Boehmer et al., 2008), Nup145C•Sec13 (Hsia et al., 2007), and Nup85•Seh1 (Brohawn et al., 2008; Debler et al., 2008) as well as associated biochemical experiments, have led to a deeper and broader understanding of how the scaffold of the NPC is assembled from its constituent parts.

The structural subunits of the NPC were initially predicted to be composed of simple combinations of regular α-helical solenoids and β-propellers (Devos et al., 2006). Experimental data now allows to specify these broad classifications, which should help to more specifically address the ancestry of the NPC. Both Sec13 and Seh1 form open, 6-bladed propellers that are completed *in trans* by the N-terminal insertion blades of their binding partners Nup145C and Nup85, respectively. Furthermore, helical nucleoporins Nic96, Nup145C, Nup85, and Nup84 are built around a common and distinct ancestral coatomer element (ACE1) shared with Sec31 of the outer coat of COPII vesicles (Brohawn et al., 2008). In ACE1 proteins, a specific N-terminal elaboration is followed by a tripartite helical domain composed of a trunk, a crown and a tail element. The ~ 30 helices within ACE1 follow a J-like pattern, zig-zagging up on one side of the trunk, making a U-turn within the crown domain, and then following down on the opposite side of the trunk (Figure 6A, right panel). The tail domain is often attached with modest flexibility to the trunk and is missing in most crystal constructs. In the case of Nup145C and Nup85 the N-terminal elaborations are the aforementioned insertion blades that bind to Sec13 and Seh1. Nup145C•Sec13 and Nup85•Seh1 heterodimers form the two proximal segments of the Y-shaped complex and are tethered together by Nup120 (Brohawn et al., 2008).

Based on structure predictions and its overall size, it was reasonable to suggest that Nup120 may take on a structure similar to Nup145C•Sec13 and Nup85•Seh1, with the only major difference being that the β-propeller and the α-helical domains are fused into one polypeptide chain. However, comparison between the structure of Nup120 and the Nup85•Seh1 heterodimer reveals a marked difference in topology (Figure 6A). Whereas the ACE1 architecture of Nup85 forms an elongated α-helical domain, the central α-helical domain of Nup120 is nearly as wide as it is long, forming an almost globular structure. The ACE1 trunk module covers the bottom face of the Seh1 β-propeller, while in Nup120 the helical domain is attached to and integrated into an edge of the β-propeller. Further, the ACE1•β-propeller interaction is accomplished by the addition of an insertion blade N-terminal to ACE1, while in Nup120 the β-propeller domain inserts a 4-helix bundle into the central α-helical domain. This helical insertion fits snugly into a pocket formed by helices α5-α7 and α11-α13 and creating an interface of nearly 600 $Å^2$ (Figure 6B).

The extensive interaction between the β-propeller and α-helical domain of Nup120 creates a large, rigid interface of 2175 $Å^2$. In contrast, the largest contact area between ACE1 and its β-propeller partner is at the insertion blade/β-propeller interface. Additional contact areas in ACE1•β-propeller complexes are smaller in comparison to the corresponding interfaces in Nup120 and, importantly, far less hydrophobic. Thus, for the ACE1•β-propeller assembly one has to consider substantial flexibility about the interaction joint, while the Nup120 structure

presented here is very likely inflexible. Not only does the structure of Nup120 significantly differ from the ACE1•β-propeller heterodimers, but additional emerging evidence suggests that it also lacks similarity to Nup170 and Nup133, the two other scaffolding nucleoporins of similar size and domain composition with an N-terminal β-propeller followed by an α-helical domain (Whittle & Schwartz, manuscript in preparation).

DISCUSSION

Here we report the crystal structure of Nup120, a large, universally conserved architectural nucleoporin. This structure adds substantially to the growing inventory of crystallographically characterized nucleoporins. As a result of these studies, we learn that the NPC is constructed from nucleoporins with a limited set of domain architectures. While other α-helical and β-propeller domains of scaffold nucleoporins fall into distinct classes, likely pointing to gene duplication in the early evolution of the NPC, the Nup120 architecture appears to be quite distinct. A search for structurally related proteins fails in detecting similarity beyond the isolated β-propeller scaffold or the arrangement of more than 6 α-helices. Within the list of crystallographically uncharacterized nucleoporins, none is likely to match the Nup120 structure closely.

Nup120 in the Context of the NPC Scaffold

Nup120 forms one of the two short arms of the universally conserved, 0.6 MDa Y-complex, the essential building block of the NPC scaffold. The assembly of the Y-complex from its 7 members is fairly well understood and has been studied using many different techniques. All of these studies profit from generally very high affinities observed between the interacting proteins within the Y, which generated largely consistent co-immunoprecipitation and yeast two-hybrid results and facilitated the crystallization of several complex crystal structures. While there is general agreement on the overall topology of the NPC, as determined by electron microscopic techniques, different models for the assembly of the NPC structural scaffold and the integration of the Y-complex are being discussed, as more detailed information is becoming available.

Based on a combination of computational, structural, biochemical, and *in vivo* experiments, a model was proposed where the Y-complex is positioned in two 8-membered rings located at the periphery of the NPC sandwiching two equally wide rings composed of Nup157/170,Nup188 and Nup192 in between (Alber et al., 2007). One exiting aspect of the combinatorial approach is, that going forward to a higher resolution it may allow the integration of crystallographic data as well, in which case it could come close to a detailed molecular description of the NPC.

Blobel and coworkers proposed a concentric cylinder model based on crystal-packing interactions where four 8-membered rings of the Y-complex are stacked and placed directly adjacent and in contact to the curved membrane (Debler et al., 2008; Hsia et al., 2007). Further, Nup85•Seh1 and Nup145C•Sec13 are both supposed to form heterooctameric fence poles spanning the NPC vertically, thereby connecting the 4 stacked rings. Nup157/170, Nup188, Nup192 and Nic96 are suggested to form a second inner layer bridging to a third layer composed of FG-nups. With a Y-complex scaffold twice the mass of the computer-generated model, the concentric cylinder model generates a densely packed NPC coat.

In contrast to the concentric cylinder model, we proposed a lattice-like model for the NPC, extrapolated from the assembly of COPII vesicle coats and substantiated by the structure and assembly principles of core components of the NPC scaffold (Brohawn et al., 2008; Brohawn and Schwartz, 2009). We propose the Y-complex does not directly coat the pore membrane (in analogy to the COPII outer coat), but is anchored by another set of proteins, likely involving

the essential transmembrane nucleoporin Ndc1 and/or its direct binding partners (Onischenko et al., 2009). It is of interest to discuss this issue in respect to the membrane-inserting ALPS motif that was experimentally characterized within a loop structure in hNup133-NTD and that was predicted to occur as well in yNup85 and yNup120 (Drin et al., 2007). Based on the structural data now available on both yNup85 and yNup120, it appears unlikely that the predicted ALPS motif in both proteins is functional in membrane-binding since neither is in an exposed region of the protein, or is likely to become exposed. This is in contrast to the ALPS motif in hNup133-NTD, where it is well exposed in the crystal structure, and also highly conserved in metazoa (Berke et al., 2004). Taking all the available data together, it appears more reasonable to suggest a specific function for the ALPS motif in metazoan Nup133 rather than a general function in anchoring of the NPC to the pore membrane. Since Nup133-ALPS is only poorly conserved in yeast, it is tempting to speculate that it may have a specific role in NPC assembly in open mitosis (Güttinger et al., 2009). We predict that the lattice scaffold of the NPC is built from edge and vertex elements, following similar assembly principles as established for COPII. However, in the absence of definitive inter-subcomplex interaction data, any detailed NPC assembly model is still premature and has to be interpreted cautiously.

The fact that inter-subunit interactions are still obscure suggests that these interactions are rather weak and hard to establish. Each short arm of the Y-complex contains one β-propeller domain, while the stalk contains two (Figure 1). For the assembly of the extensions of the Y, direct interactions between the α-helical domains is essential, however this does not exclude the participation of the β-propellers. It is reasonable to suggest, that the β-propellers are prime candidates for the elusive inter-subcomplex contacts. The vertices of the outer coat of COPII vesicles are assembled exclusively via β-propeller interactions, which have still only been inferred by fitting crystal structures into EM maps (Fath et al., 2007;Stagg et al., 2008). β-propellers make excellent protein-protein interfaces due to their inherent ability to pair with a binding partner in multiple modes. Binding to peptides via the face of the β-propeller is well known (Jawad and Paoli, 2002). Additionally, each blade exposes on its edge (typically on strand D) a stretch of ~ 6-8 residues available for intermolecular β-sheet formation, which can be likened to one half of a zipper. In Nup120, 5 of the 7 blades are exposed this way, two are buried in the hydrophobic core shared with the attached α-helical domain. In addition to these interactions being relatively weak, another inherent difficulty in identifying them is that they are likely very poorly conserved at the sequence level because the contacts are mediated via the backbone rather than side chains. Based on the available data, it is conceivable that the Nup120 β-propeller is involved in inter-Y contacts. It is also possible that it is used to bridge to the Nic96 complex, but we can also not exclude that it may be an anchor for dynamic nucleoporins or other accessory proteins. The relatively mild *nup120Δ* phenotype (Figure 5) compared to *nup133Δ or nup84Δ* and the behavior of $Nup120_{1\text{-}757}$-GFP suggests that if the Nup120 β-propeller has an integral role in the NPC scaffold, it is either redundant or can be functionally replaced by another nucleoporin.

In summary, we show that Nup120 adopts a unique architecture to build one of the two arms of the multimeric Y-shaped complex, the linchpin of the NPC scaffold. The atomic structure of the universally conserved heptameric core of the Y complex is now nearing completion. With reliable data on inter-subcomplex contacts the construction of a basic NPC architecture is within reach in the close future.

EXPERIMENTAL PROCEDURES

Protein Expression and Purification

Nup120 from *S. cerevisiae* (residues 1-757 of 1037) was expressed at 18°C in *E. coli* strain BL21(DE3)-RIL as a 6xHis N-terminal fusion protein from a pET-Duet-derived plasmid. Cells were pelleted and resuspended in lysis buffer (50mM potassium phosphate pH 8.0, 500mM

NaCl, 40mM imidazole, 5mM β-mercaptoethanol). Cells were lysed using a french press and the clear lysate incubated in batch with Ni-affinity resin. After washing the resin in batch with lysis buffer, the protein was eluted with lysis buffer containing 250mM imidazole. After cleavage of the purification tag, Nup120 was subjected to size exclusion chromatography on Superdex S200 equilibrated in 10mM Tris/HCl pH 8.0, 150mM NaCl, 0.1mM EDTA, and 1mM DTT. Nup120 eluted as a monomer of 88 kDa. Selenomethionine-derivatized protein was prepared as previously described (Brohawn et al., 2008) and Nup120-SeMet was purified identically to the native version.

Full length Nup85 in complex with Seh1 and a single chain version of full-length Nup145C in complex with Sec13 from *S.cerevisiae* were cloned as described (Brohawn et al., 2008), purified as for Nup120 (residues 1-757), and are referred to in the text as Nup85•Seh1 and Nup145C•Sec13. The C-terminal helical domain of Nup120 (residues 766-1037) was generated from a full length Nup120 construct by PCR. A 5-protein complex of Nup120 (residues 766-1037), Nup85•Seh1, and Nup145C•Sec13 was prepared by co-expression of a trimeric complex of Nup120 (residues 766-1037)•Nup85•Seh1 (Brohawn et al., 2008) and the single chain version of Nup145C•Sec13 in BL21(DE3)-(RIL) cells and was purified as for Nup120 (residues 1-757). The Ni-NTA elution was pooled, digested with human rhinovirus 3C to remove fusion tags, and subjected to size exclusion chromatography using a Superdex S200 26/60 column equilibrated in 10mM Tris/HCl pH 8.0, 250mM NaCl, 1mM DTT, and 0.1mM EDTA.

Protein Crystallization

Nup120 concentrated to 20 mg/ml was crystallized in 15% (w/v) PEG 3350, and 0.1M Tris/HCl pH 7.5, 0.2M KSCN by the hanging drop vapor diffusion method at 18°C in 2μl drops. Crystals grew within 3-6 days forming rhomboid prisms with dimensions of 60μm × 60μm × 20μm. The selenomethionine derivative crystallized in the same condition, while the highest quality crystals were obtained by microseeding with native crystals. Both native and derivative crystals were cryo-protected by serial transfer of the crystals into reservoir solutions supplemented with increasing amounts of PEG200 (10%-25% (v/v), 5% steps) before flash freezing in liquid nitrogen. Both native and derivative protein crystallized in space group $P2_12_12$ with one molecule per asymmetric unit. Data was collected at beamline 24ID-C at Argonne National Laboratory.

Structure Determination

Although the native crystals were larger and optically superior, the selenomethionine-derivatized crystals diffracted significantly better and were exclusively used for data analysis. A complete dataset was collected at the Se-Peak wavelength and data reduction was carried out using the HKL2000 package (Otwinowski and Minor, 1997). All 9 selenium sites were found using SHELXD (Sheldrick, 2008). After refinement of the Se positions and density modification with SHARP, an adequate experimental electron density map was obtained, allowing for the assignment and building of the majority of the structure. Sequence assignment was aided by using the selenium positions as markers. Model building was done with Coot (Emsley and Cowtan, 2004) and refinement was carried out using the PHENIX suite (Adams et al., 2002). The model is complete except for residues 31-52, 188-200, 303-313, and 731-757 for which only spurious electron density was observed. Blades 3 and 4 of the β-propeller have the highest temperature factors and are not as well packed as the remainder of the molecule. Sequence assignment in this region, particularly in strand 3D residues 204-216, is tentative.

Analytical Size Exclusion Chromatography

For Nup120 (residues 1-757), Nup145C•Sec13, and Nup85•Seh1 binding experiments, equimolar amounts of each component were incubated alone or in combination for 30 minutes

at 4°C in binding buffer (10mM Tris/HCl pH 8.0, 250mM NaCl, 1mM DTT, 0.1mM EDTA). Reactions were injected onto a Superdex S200 hr10/300 column (GE Healthcare) equilibrated in binding buffer, and run at a flow rate of 0.8 ml/min (Figure 4A).

Yeast Strain Construction

Deletion strains were taken from the Yeast Deletion Consortium (Winzeler et al., 1999), C-terminal GFP-tagging was done by homologous recombination in a BY4741 background, using pFA6a-GFP(S65T)-kanMX6 as template for C-terminal modifications (Longtine et al., 1998). Strains were selected on G418 plates (200 μg/ml) and verified by PCR.

Fluorescence Microscopy

Strains were grown overnight in YPD (1% yeast extract, 2% yeast peptone, 2% glucose) at 30° C, diluted 20-fold into fresh YPD, and grown for 4-5 hours at 30°C to OD_{600} ~0.5. Cells were harvested by centrifugation, fixed for 3 minutes in 3.7% formaldehyde/0.1M potassium phosphate pH 6.5, and prepared for immunofluorescence as previously described (Kilmartin and Adams, 1984). Samples were incubated with mAb414 (abcam, 1:1000) alone or in combination with goat anti-GFP (1:500) for 90 minutes at room temperature. Bound antibodies were detected by incubation with Cy5-conjugated anti-mouse (Jackson Labs, 1:500) alone or in combination with Cy2-conjugated donkey anti-goat (Jackson Labs, 1:200) for 45 minutes at room temperature. DNA was stained with 0.05 μg/ml 4′,6-diamidino-2-phenylindole (Sigma-Aldrich) and samples were mounted for imaging in 1 mg/ml p-phenylenediamine and 90% glycerol. Fluorescence microscopy was performed on a Zeiss AxioImager.Z1 microscope and images were taken with a Zeiss AxioCam HRm camera.

ACKNOWLEDGEMENTS

We thank staff at the NE-CAT beamline 24 at Argonne National Laboratory for excellent assistance with data collection; Iain Cheeseman for providing antibodies; Eric Spear for advice on *in vivo* experiments; Dennis Kim for use of his fluorescence microscope. Supported by NIH Grant GM77537 (T.U.S.), a Pew Scholar Award (T.U.S.), a Koch Fellowship Award (S.G.B.) and a Vertex Scholarship (S.G.B.).

REFERENCES

Adams PD, Grosse-Kunstleve RW, Hung LW, Ioerger TR, McCoy AJ, Moriarty NW, Read RJ, Sacchettini JC, Sauter NK, Terwilliger TC. PHENIX: building new software for automated crystallographic structure determination. Acta Crystallogr D Biol Crystallogr 2002;58:1948–1954. [PubMed: 12393927]

Aitchison JD, Blobel G, Rout MP. Nup120p: a yeast nucleoporin required for NPC distribution and mRNA transport. J. Cell Biol 1995;131:1659–1675. [PubMed: 8557736]

Alber F, Dokudovskaya S, Veenhoff LM, Zhang W, Kipper J, Devos D, Suprapto A, Karni-Schmidt O, Williams R, Chait BT, et al. The molecular architecture of the nuclear pore complex. Nature 2007;450:695–701. [PubMed: 18046406]

Aris JP, Blobel G. Yeast nuclear envelope proteins cross react with an antibody against mammalian pore complex proteins. J. Cell Biol 1989;108:2059–2067. [PubMed: 2661560]

Beck M, Lucic V, Forster F, Baumeister W, Medalia O. Snapshots of nuclear pore complexes in action captured by cryo-electron tomography. Nature 2007;449:611–615. [PubMed: 17851530]

Berke IC, Boehmer T, Blobel G, Schwartz TU. Structural and functional analysis of Nup133 domains reveals modular building blocks of the nuclear pore complex. J. Cell Biol 2004;167:591–597. [PubMed: 15557116]

Boehmer T, Jeudy S, Berke IC, Schwartz TU. Structural and functional studies of Nup107/Nup133 interaction and its implications for the architecture of the nuclear pore complex. Mol. Cell 2008;30:721–731. [PubMed: 18570875]

Brohawn SG, Leksa NC, Spear ED, Rajashankar KR, Schwartz TU. Structural evidence for common ancestry of the nuclear pore complex and vesicle coats. Science 2008;322:1369–1373. [PubMed: 18974315]

Brohawn SG, Schwartz TU. A lattice model of the nuclear pore complex. Comm. & Integr. Biol 2009;2:1–3.

Chaudhuri I, Soding J, Lupas AN. Evolution of the beta-propeller fold. Proteins 2008;71:795–803. [PubMed: 17979191]

Cronshaw JM, Krutchinsky AN, Zhang W, Chait BT, Matunis MJ. Proteomic analysis of the mammalian nuclear pore complex. J. Cell Biol 2002;158:915–927. [PubMed: 12196509]

D'Angelo MA, Hetzer MW. Structure, dynamics and function of nuclear pore complexes. Trends Cell Biol 2008;18:456–466. [PubMed: 18786826]

D'Angelo MA, Raices M, Panowski SH, Hetzer MW. Age-dependent deterioration of nuclear pore complexes causes a loss of nuclear integrity in postmitotic cells. Cell 2009;136:284–295. [PubMed: 19167330]

Debler EW, Ma Y, Seo HS, Hsia KC, Noriega TR, Blobel G, Hoelz A. A fence-like coat for the nuclear pore membrane. Mol. Cell 2008;32:815–826. [PubMed: 19111661]

Devos D, Dokudovskaya S, Williams R, Alber F, Eswar N, Chait BT, Rout MP, Sali A. Simple fold composition and modular architecture of the nuclear pore complex. Proc. Natl. Acad. Sci. U S A 2006;103:2172–2177. [PubMed: 16461911]

Drin G, Cassella J-F, Gautier R, Boehmer T, Schwartz TU, Antonny B. A general amphipathic α-helixcal motif for sensing membrane curvature. Nat. Struct. Mol. Biol 2007;14:138–146. [PubMed: 17220896]

Emsley P, Cowtan K. Coot: model-building tools for molecular graphics. Acta Crystallogr. D Biol. Crystallogr 2004;60:2126–2132. [PubMed: 15572765]

Fath S, Mancias JD, Bi X, Goldberg J. Structure and Organization of Coat Proteins in the COPII Cage. Cell 2007;129:1325–1336. [PubMed: 17604721]

Gillespie PJ, Khoudoli GA, Stewart G, Swedlow JR, Blow JJ. ELYS/MEL-28 chromatin association coordinates nuclear pore complex assembly and replication licensing. Curr. Biol 2007;17:1657–1662. [PubMed: 17825564]

Güttinger S, Laurell E, Kutay U. Orchestrating nuclear envelope disassembly and reassembly during mitosis. Nat. Rev. Mol. Cell. Biol 2009;10:178–191. [PubMed: 19234477]

Harel A, Orjalo AV, Vincent T, Lachish-Zalait A, Vasu S, Shah S, Zimmerman E, Elbaum M, Forbes DJ. Removal of a single pore subcomplex results in vertebrate nuclei devoid of nuclear pores. Mol. Cell 2003;11:853–864. [PubMed: 12718872]

Hawryluk-Gara LA, Platani M, Santarella R, Wozniak RW, Mattaj IW. Nup53 is required for nuclear envelope and nuclear pore complex assembly. Mol. Biol. Cell 2008;19:1753–1762. [PubMed: 18256286]

Heath CV, Copeland CS, Amberg DC, Del Priore V, Snyder M, Cole CN. Nuclear pore complex clustering and nuclear accumulation of poly(A)+ RNA associated with mutation of the Saccharomyces cerevisiae RAT2/NUP120 gene. J. Cell Biol 1995;131:1677–1697. [PubMed: 8557737]

Hsia KC, Stavropoulos P, Blobel G, Hoelz A. Architecture of a coat for the nuclear pore membrane. Cell 2007;131:1313–1326. [PubMed: 18160040]

Jawad Z, Paoli M. Novel sequences propel familiar folds. Structure 2002;10:447–454. [PubMed: 11937049]

Jeudy S, Schwartz TU. Crystal structure of nucleoporin Nic96 reveals a novel, intricate helical domain architecture. J. Biol. Chem 2007;282:34904–34912. [PubMed: 17897938]

Kilmartin JV, Adams AE. Structural rearrangements of tubulin and actin during the cell cycle of the yeast Saccharomyces. J. Cell Biol 1984;98:922–933. [PubMed: 6365930]

Li O, Heath CV, Amberg DC, Dockendorff TC, Copeland CS, Snyder M, Cole CN. Mutation or deletion of the Saccharomyces cerevisiae RAT3/NUP133 gene causes temperature-dependent nuclear accumulation of poly(A)+ RNA and constitutive clustering of nuclear pore complexes. Mol. Biol. Cell 1995;6:401–417. [PubMed: 7626806]

Lim RY, Ullman KS, Fahrenkrog B. Biology and biophysics of the nuclear pore complex and its components. Int. Rev. Cell Mol. Biol 2008;267:299–342. [PubMed: 18544502]

Liu HL, De Souza CP, Osmani AH, Osmani SA. The three fungal transmembrane nuclear pore complex proteins of Aspergillus nidulans are dispensable in the presence of an intact An-Nup84-120 complex. Mol. Biol. Cell 2009;20:616–630. [PubMed: 19019988]

Liu Y, Eisenberg D. 3D domain swapping: as domains continue to swap. Protein Sci 2002;11:1285–1299. [PubMed: 12021428]

Loiodice I, Alves A, Rabut G, Van Overbeek M, Ellenberg J, Sibarita JB, Doye V. The entire Nup107-160 complex, including three new members, is targeted as one entity to kinetochores in mitosis. Mol. Biol. Cell 2004;15:3333–3344. [PubMed: 15146057]

Longtine MS, McKenzie A 3rd, Demarini DJ, Shah NG, Wach A, Brachat A, Philippsen P, Pringle JR. Additional modules for versatile and economical PCR-based gene deletion and modification in Saccharomyces cerevisiae. Yeast 1998;14:953–961. [PubMed: 9717241]

Lutzmann M, Kunze R, Buerer A, Aebi U, Hurt E. Modular self-assembly of a Y-shaped multiprotein complex from seven nucleoporins. EMBO J 2002;21:387–397. [PubMed: 11823431]

Marelli M, Aitchison JD, Wozniak RW. Specific binding of the karyopherin Kap121p to a subunit of the nuclear pore complex containing Nup53p, Nup59p, and Nup170p. J. Cell Biol 1998;143:1813–1830. [PubMed: 9864357]

Onischenko E, Stanton LH, Madrid AS, Kieselbach T, Weis K. Role of the Ndc1 interaction network in yeast nuclear pore complex assembly and maintenance. J. Cell Biol 2009;185:475–491. [PubMed: 19414609]

Otwinowski Z, Minor W. Processing of X-ray diffraction data collected in oscillation mode. Methods Enzymol 1997;276:307–326.

Pemberton LF, Rout MP, Blobel G. Disruption of the nucleoporin gene NUP133 results in clustering of nuclear pore complexes. Proc. Natl. Acad. Sci. U S A 1995;92:1187–1191. [PubMed: 7862658]

Rabut G, Doye V, Ellenberg J. Mapping the dynamic organization of the nuclear pore complex inside single living cells. Nat. Cell Biol 2004;6:1114–1121. [PubMed: 15502822]

Rasala BA, Orjalo AV, Shen Z, Briggs S, Forbes DJ. ELYS is a dual nucleoporin/kinetochore protein required for nuclear pore assembly and proper cell division. Proc. Natl. Acad. Sci. U S A 2006;103:17801–17806. [PubMed: 17098863]

Schrader N, Stelter P, Flemming D, Kunze R, Hurt E, Vetter IR. Structural Basis of the Nic96 Subcomplex Organization in the Nuclear Pore Channel. Mol. Cell 2008;29:46–55. [PubMed: 18206968]

Schwartz TU. Modularity within the architecture of the nuclear pore complex. Curr. Opin. Struct. Biol 2005;15:221–226. [PubMed: 15837182]

Sheldrick GM. A short history of SHELX. Acta Crystallographica 2008;64:112–122. [PubMed: 18156677]

Siniossoglou S, Lutzmann M, Santos-Rosa H, Leonard K, Mueller S, Aebi U, Hurt E. Structure and assembly of the Nup84p complex. J. Cell Biol 2000;149:41–54. [PubMed: 10747086]

Siniossoglou S, Wimmer C, Rieger M, Doye V, Tekotte H, Weise C, Emig S, Segref A, Hurt EC. A novel complex of nucleoporins, which includes Sec13p and a Sec13p homolog, is essential for normal nuclear pores. Cell 1996;84:265–275. [PubMed: 8565072]

Stagg SM, LaPointe P, Razvi A, Gurkan C, Potter CS, Carragher B, Balch WE. Structural basis for cargo regulation of COPII coat assembly. Cell 2008;134:474–484. [PubMed: 18692470]

Stoffler D, Feja B, Fahrenkrog B, Walz J, Typke D, Aebi U. Cryo-electron tomography provides novel insights into nuclear pore architecture: implications for nucleocytoplasmic transport. J Mol. Biol 2003;328:119–130. [PubMed: 12684002]

Tran EJ, Wente SR. Dynamic nuclear pore complexes: life on the edge. Cell 2006;125:1041–1053. [PubMed: 16777596]

Walther TC, Alves A, Pickersgill H, Loiodice I, Hetzer M, Galy V, Hulsmann BB, Kocher T, Wilm M, Allen T, et al. The conserved Nup107-160 complex is critical for nuclear pore complex assembly. Cell 2003;113:195–206. [PubMed: 12705868]

Wang H, Kakaradov B, Collins SR, Karotki L, Fiedler D, Shales M, Shokat KM, Walther T, Krogan NJ, Koller D. A complex-based reconstruction of the S. cerevisiae interactome. Mol. Cell Proteomics. 2009epub ahead of print

Weis K. Regulating access to the genome: nucleocytoplasmic transport throughout the cell cycle. Cell 2003;112:441–451. [PubMed: 12600309]

Winzeler EA, Shoemaker DD, Astromoff A, Liang H, Anderson K, Andre B, Bangham R, Benito R, Boeke JD, Bussey H, et al. Functional characterization of the S. cerevisiae genome by gene deletion and parallel analysis. Science 1999;285:901–906. [PubMed: 10436161]

Yu H, Braun P, Yildirim MA, Lemmens I, Venkatesan K, Sahalie J, Hirozane-Kishikawa T, Gebreab F, Li N, Simonis N, et al. High-quality binary protein interaction map of the yeast interactome network. Science 2008;322:104–110. [PubMed: 18719252]

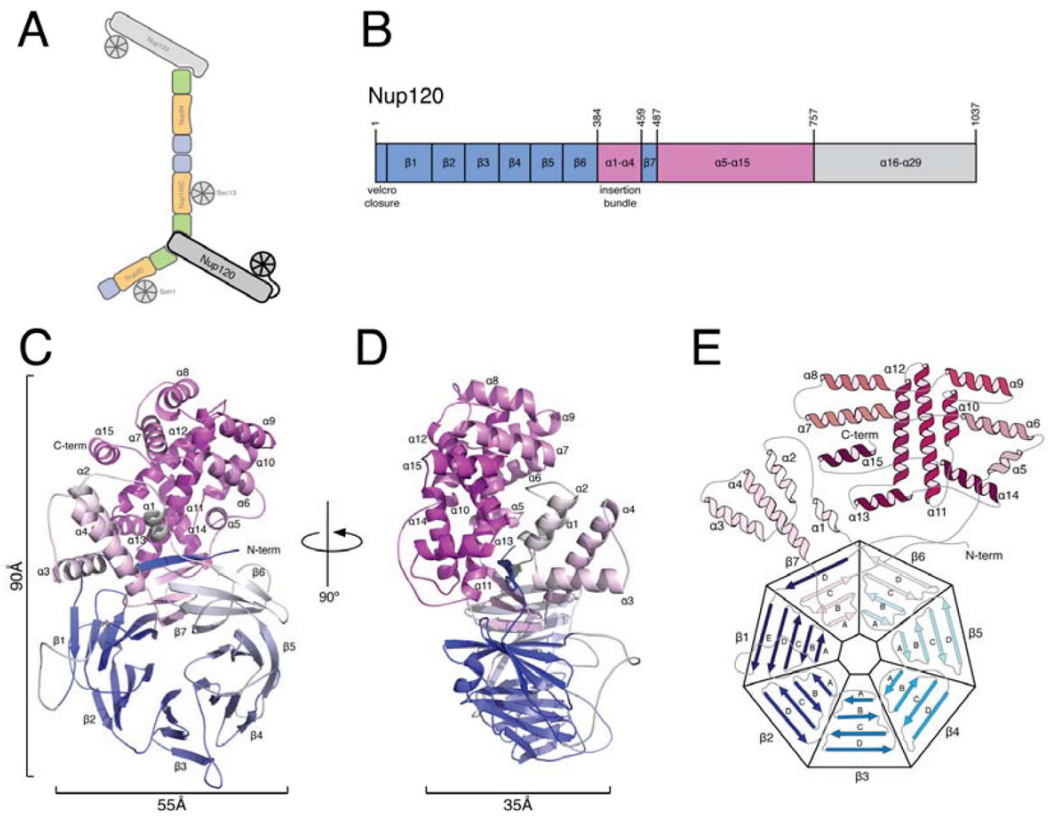

Figure 1. Overall Topology of Nup120

(A) Current model of the Y-shaped Nup84 subcomplex. The relative position of Nup120 is highlighted. (B) Schematic of full-length Nup120 from *S. cerevisiae*. Residues that form the β-propeller are colored blue, those that form the α-helical domain are purple, and those not present in the crystallized construct are in gray. (C, D) The overall topology of Nup120 (residues 1-757 of 1037) is shown in two views rotated by 90°. The structure is gradient-colored from blue to white to magenta from N- to C-terminus. At its N-terminus, Nup120 forms a 7-bladed β-propeller. A 4-helix bundle (α1-α4) between blades 6 and 7 packs against the remainder of the helical domain (α5-α15), composed of helices wrapping around a central hydrophobic stalk of the two long helices α11 and α12. Unstructured loops absent from the final model are shown in gray. (E) A topological diagram of the Nup120 structure is shown, illustrating the 4-helix insertion between blades 6 and 7 of the propeller as well as the two central helices of the helical domain.

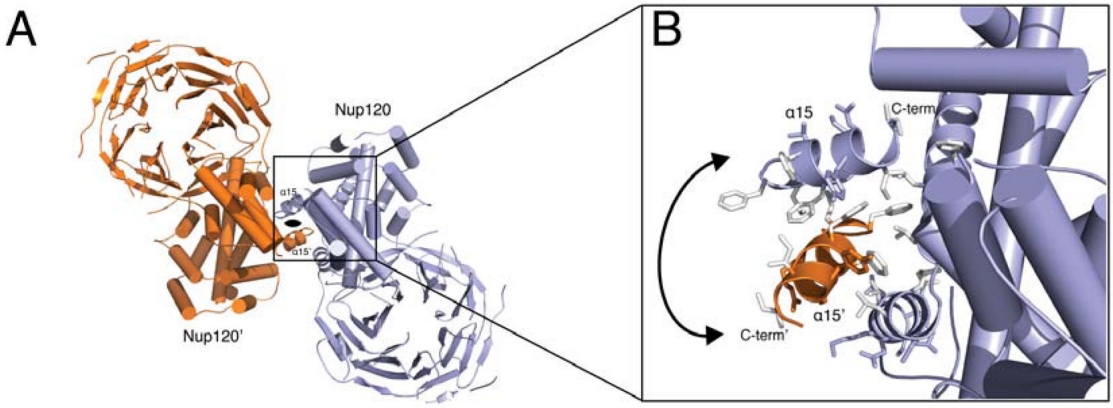

Figure 2. Crystal Contacts between Two Symmetry-Related Molecules

(A) One molecule of Nup120 in blue, and its symmetry mate, related by a 2-fold rotation, in orange. The β-propellers are at opposite ends while the helical domains engage in a putative domain swap between helices α15 of both molecules. (B) Close-up of the domain-swapped region, illustrating the hydrophobic nature of helix α15 and the surrounding pocket (hydrophobic residues are shown in white). In monomeric Nup120, helix α15 likely folds under (arrow) and occupies the position taken by helix α15′ (orange) of the symmetry-related molecule in the crystal.

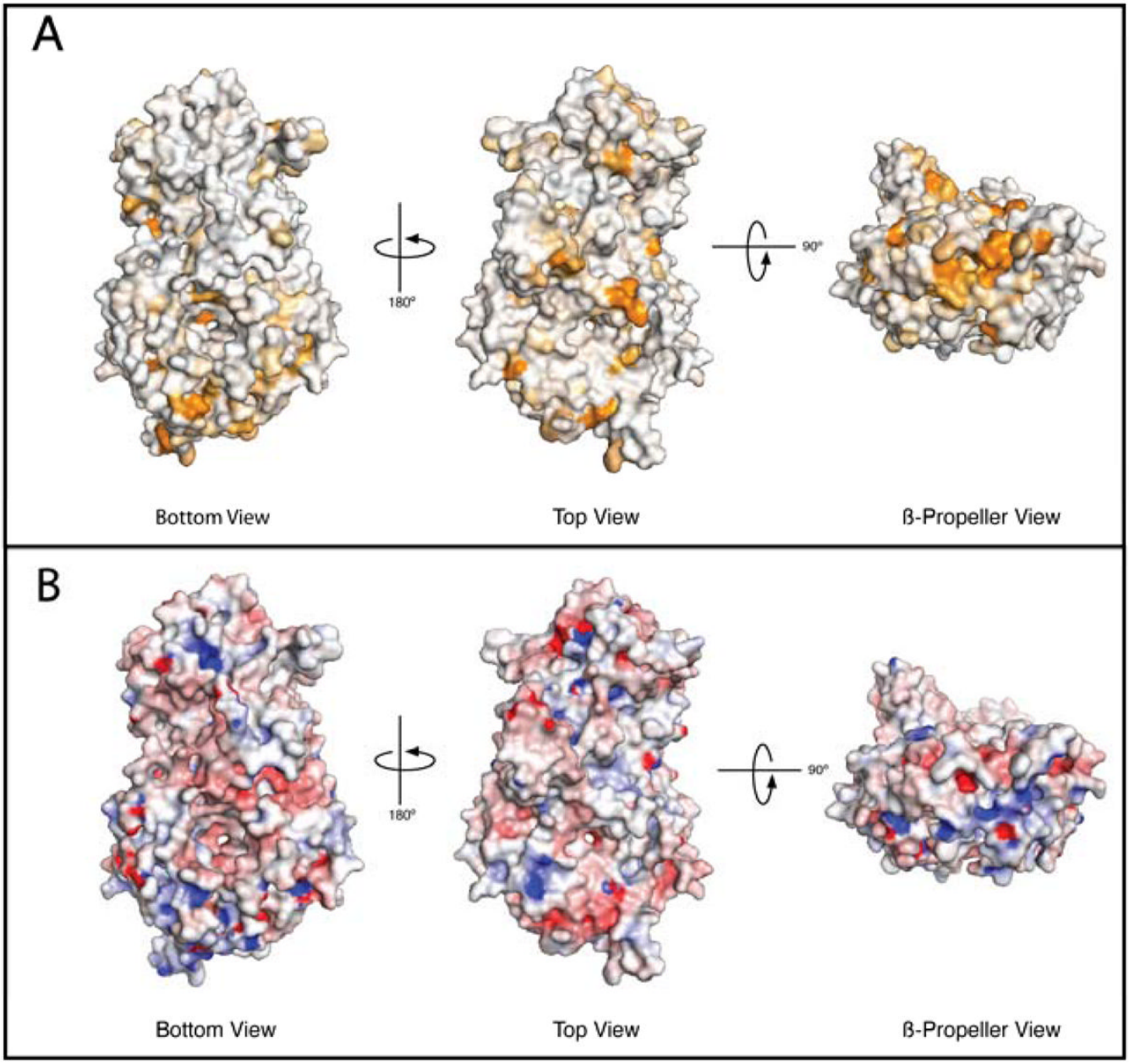

Figure 3. Surface Conservation and Electrostatics of Nup120

(A) Surface conservation of Nup120 is shown from three different views. To illustrate the conservation of residues on the surface of Nup120, a multiple sequence alignment sampling the phylogenetic tree of budding yeasts was generated and mapped onto the surface, colored from white (not conserved) to orange (highly conserved). The view in the middle panel corresponds to the view shown in Figure 1C. A patch of highly conserved residues is apparent on the outer face of the propeller domain of Nup120. (B) The electrostatic surface potential of Nup120 is shown in the same views as in (A) and is colored from red (−10 kT/e) to blue (+10 kT/e).

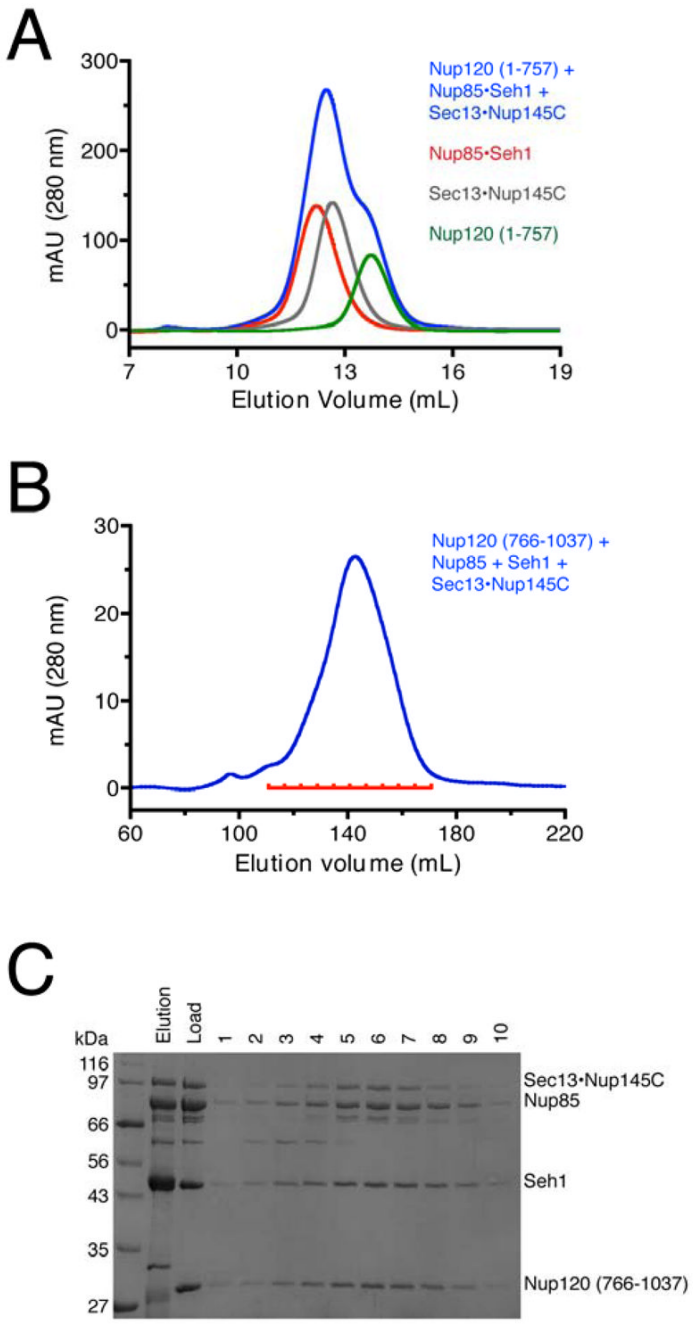

Figure 4. The C-Terminus of Nup120 Is Necessary for Binding Nup85 •Seh1 and Nup145C•Sec13

(A) Nup85•Seh1 (red), Nup145C•Sec13 (gray), and $Nup120_{1-757}$ (green) were run individually and in combination (blue) on a Superdex S200 10/300 gelfiltration column. (B) Nup85•Seh1, Nup145C•Sec13, and $Nup120_{766-1037}$ were incubated together and run on Superdex S200 26/60 and eluted in a single peak. (C) Fractions from the gel filtration experiment in B were analyzed by SDS-Page. Co-migration of Nup85•Seh1, Nup145C•Sec13, and $Nup120_{766-1037}$ indicates that the C-terminus of Nup120 is necessary for the formation of the pentameric complex that comprises the hub of the Y-shaped complex.

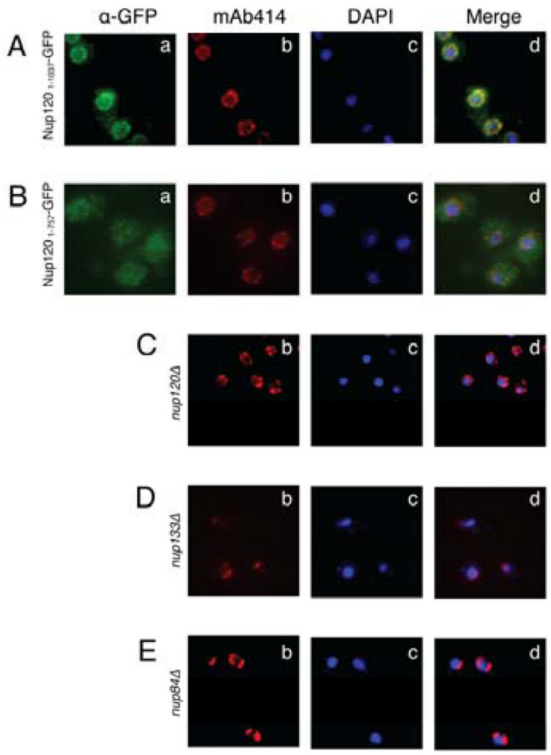

Figure 5. Nup120$_{1-757}$ Does Not Localize to the Nuclear Envelope

(Aa-Ad) Nup120-GFP is targeted to the nuclear envelope, as confirmed by co-localization with mAb414 (staining FG-Nups), while Nup120$_{1-757}$-GFP (Ba-Bd) is distributed throughout the cell. Mislocalization indicates that the C-terminus of Nup120 is necessary for proper recruitment to the NPC. *Nup120Δ*, *nup133Δ*, and *nup84Δ* cells (in the same BY4741 strain background) are shown for comparison (Cb-Cd, Db-Dd, Eb-Ed). Nuclear rim was visualized using mAb414, GFP-tagged Nup120 using goat α-GFP, and DNA using DAPI. Merged images are shown on the right.

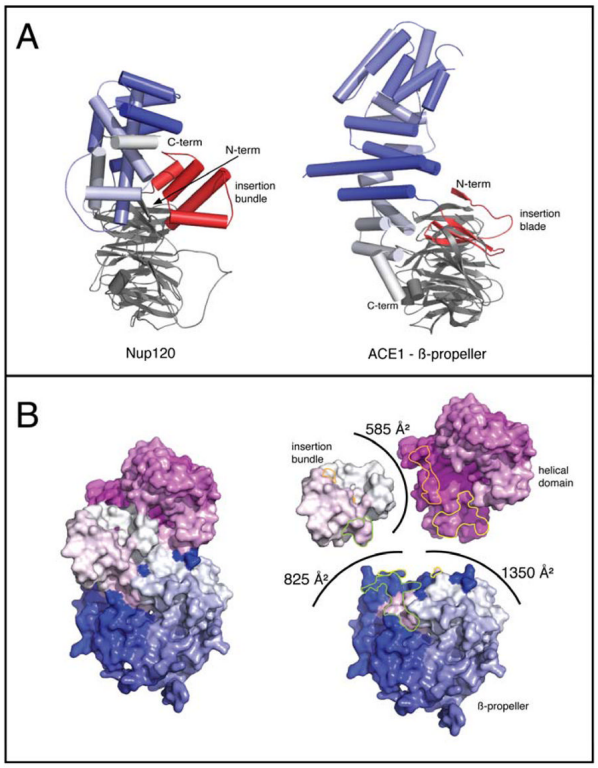

Figure 6. Nup120 is Composed of a combined β-Propeller - α-Helical Domain distinct from ACE1•β-Propeller

(A) The overall architectures of Nup120 and the ACE1 motif of Nup85•Seh1 are distinctly different. Nup120 is characterized by a bipartite helical domain (blue to white from N- to C-terminus) that is interrupted by a β-propeller domain (gray). The Nup85 ACE1 motif is characterized by an elongated helical stack (colored blue to white from N- to C-terminus) that makes a U-turn in the crown domain of the molecule. At its N-terminus, Nup85 inserts a blade (in red) into the open, 6-bladed Seh1 β-propeller. In contrast, the β-propeller of Nup120 contributes a helical insertion bundle (red) to the helical domain. The view of Nup120 is the same as that in Fig. 3B. (B) Surface representations of intact Nup120 are shown on the left, while on the right the three modules of Nup120 – the propeller, the helical insertion, and the helical domain – are shown pulled apart to illustrate the buried surface areas in between. Interacting surfaces between the propeller and the insertion bundle are outlined in green, between the propeller and the helical domain in yellow, and between the insertion bundle and the helical domain in orange. The molecule is N-to-C gradient-colored from blue-to-white-to-magenta.

Table 1

Data Collection and Refinement Statistics

Data Set	**Nup120$_{1-757}$ SeMet**
Data Collection	
Space group	$P2_12_12$
Cell dimensions	
a, b, c (Å)	114.6, 153.7, 53.0
α, β, γ (°)	90.0, 90.0, 90.0
No. of unique reflections	35895
Resolution (Å)	50 - 3.0 (3.1-3.0)
R_{sym} [a] (%)	5.1
Completeness (%)	99.8 (99.6)
Redundancy	3.0 (3.0)
I/σ	20.4 (1.8)
Refinement	
Resolution (Å)	50 - 3.0
No. of unique reflections	35841
No. atoms	
Protein	5305
Water	0
R_{work} [b]	24.4
R_{free} [c]	29.9
RMSD Bond lengths (Å)	0.017
RMSD Bond angles (°)	1.915
B factor (Å^2)	
β-propeller	114
α-helical insertion bundle	89
α-helical domain	83
Ramachandran plot (%)[d]	
favored/allowed/outliers	93.61/5.3/1.09

[a] $R_{sym} = |I_i - I_i|/I_i$, where I_i is the intensity of the ith observation and I_i is the mean intensity of the reflection

[b] $R_{work} = (||F_{obs}| - |F_{calc}||/|F_{obs}|)$

[c] R_{free} = R value for a randomly selected subset (5%) of the data that were not used for minimization of the crystallographic residual

[d] Calculated using MolProbity